1521-009X/46/12/1900–1907$35.00
Drug Metabolism and Disposition

https://doi.org/10.1124/dmd.118.081893
Drug Metab Dispos 46:1900–1907, December 2018

Toward a Combinatorial Approach for the Prediction of IgG Half-Life and Clearance

Dennis R. Goulet, Michael J. Watson, Susan H. Tam, Adam Zwolak, Mark L. Chiu, William M. Atkins, and Abhinav Nath

Department of Medicinal Chemistry, University of Washington, Seattle, Washington (D.R.G., M.J.W., W.M.A., A.N.); and Biologics Research, Janssen Research and Development, LLC, Spring House, Pennsylvania (S.H.T., A.Z., M.L.C.)

Received April 6, 2018; accepted September 10, 2018

ABSTRACT

The serum half-life and clearance of therapeutic monoclonal antibodies (mAbs) are critical factors that impact their efficacy and optimal dosing regimen. The pH-dependent binding of an mAb to the neonatal Fc receptor (FcRn) has long been recognized as an important determinant of its pharmacokinetics. However, FcRn affinity alone is not a reliable predictor of mAb half-life, suggesting that other biologic or biophysical mechanisms must be accounted for. mAb thermal stability, which reflects its unfolding and aggregation propensities, may also relate to its pharmacokinetic properties. However, no rigorous statistical regression methods have been used to identify combinations of physical parameters that best predict biologic properties. In this work, a panel of eight mAbs with published human pharmacokinetic data were selected for biophysical analyses of FcRn binding and thermal stability. Biolayer interferometry was used to characterize FcRn/mAb binding at acidic and neutral pH, while differential scanning calorimetry was used to determine thermodynamic unfolding parameters. Individual binding or stability parameters were generally weakly correlated with half-life and clearance values. Least absolute shrinkage and selection operator regression was used to identify the combination of two parameters with the best correlation to half-life and clearance as being the FcRn binding response at pH 7.0 and the change in heat capacity. Leave-one-out subsampling yielded a root mean square difference between observed and predicted half-life of just 2.7 days (16%). Thus, the incorporation of multiple biophysical parameters into a cohesive model may facilitate early-stage prediction of in vivo half-life and clearance based on simple in vitro experiments.

Introduction

Monoclonal antibodies (mAbs) are an important class of drugs that have proven invaluable for the treatment of cancer, autoimmune disease, and other indications. In 2017, 10 mAb-based drugs were approved by the US Food and Drug Administration (FDA), and over 50 mAbs were in late-stage clinical trials (Kaplon and Reichert, 2018). The ability to design a wide range of agonistic or antagonistic drugs that target any soluble or cell-surface antigen, while conserving a well-defined protein scaffold, makes mAbs extremely attractive as therapeutic agents. Engineered mAb-based molecules such as bispecific antibodies and antibody-drug conjugates have introduced novel mechanisms for the treatment of disease (Spiess et al., 2015; Beck et al., 2017).

One reason for the success of mAb therapeutics, particularly of the IgG class, is their slow elimination kinetics. The serum stability of IgG mAbs makes intravenous or subcutaneous administration a feasible approach, as drug can be delivered with a dosing interval of several weeks. The biologic mechanism for the slow clearance of IgGs relies on escape from lysosomal degradation by binding to the neonatal crystallizable fragment (Fc) receptor (FcRn) via the Fc of the mAb constant region (Roopenian et al., 2003; Roopenian and Akilesh, 2007). When serum proteins are pinocytosed by endothelial cells for lysosomal proteolysis, the acidic pH of the endosome ($pH < 6.5$) allows IgG mAbs to bind FcRn located in the endosomal membrane. The complex is then trafficked back to the cell surface, where mAbs are released at the neutral pH (pH 7.4) of the blood. Thus, the importance of pH-dependent FcRn binding has long been recognized as an important determinant of IgG half-life (Raghavan et al., 1995).

Although mAbs have an average elimination half-life of several weeks in humans, there is a large variability associated with this parameter. It is not uncommon for IgG mAbs to have half-lives as short as 1 week or as long as 4 weeks (Suzuki et al., 2010; Tam et al., 2013). Mutation of the FcRn binding interface can further broaden the range of IgG clearance parameters (Robbie et al., 2013). Part of the variation in IgG half-life can be attributed to target-dependent effects, such as receptor-mediated internalization and degradation (Wang et al., 2008). However, even mAbs that target soluble antigens and lack receptor-mediated clearance have a wide range of elimination kinetics. A consequence of this variation is the investment in mAb candidates that

This work was supported by the University of Washington Department of Medicinal Chemistry; the University of Washington SOP Faculty Innovation Fund; and the National Institute of General Medical Sciences of the National Institutes of Health [Grant T32GM007750]. The content is solely the responsibility of the authors and does not necessarily represent the official views of the National Institutes of Health.

https://doi.org/10.1124/dmd.118.081893.

This article has supplemental material available at dmd.aspetjournals.org.

ABBREVIATIONS: BLI, biolayer interferometry; ΔC_P, change in heat capacity upon unfolding; ΔH, change in enthalpy of unfolding; DSC, differential scanning calorimetry; Fc, crystallizable fragment; FcRn, neonatal crystallizable fragment receptor; FDA, Food and Drug Administration; k_a, kinetic association rate constant; k_d, kinetic dissociation rate constant; LASSO, least absolute shrinkage and selection operator; mAb, monoclonal antibody; PBS, phosphate-buffered saline; PK, pharmacokinetics; RMSD, root mean square difference; T_m, melting temperature.

have suboptimal pharmacokinetic (PK) parameters, which necessitates higher doses or more frequent dosing.

To increase the convenience and cost-effectiveness of mAb therapies, there is a need for predictive models that can accurately determine PK properties before candidates are investigated in animals or humans. Ideally, these models would be based on biophysical parameters that can be readily measured early in the drug pipeline (Dostalek et al., 2017; Avery et al., 2018). Historically, FcRn binding at endosomal and neutral pH have both been shown to affect mAb elimination, and accounting for the interaction at both pH values may provide more predictive success (Wang et al., 2011; Souders et al., 2015). Thermal stability, and related properties like aggregation propensity, may also affect half-life, although less is known about this possible relationship (Datta-Mannan et al., 2015a). Although these and other biophysical parameters, such as nonspecific binding or electrostatic interactions, may be predictively important (Datta-Mannan et al., 2015b; Tibbitts et al., 2016; Jain et al., 2017), their relative contributions and the underlying mechanistic relationships remain unclear.

In this work, we characterized the FcRn binding properties and thermal stability of a panel of IgG1 mAbs and, using the LASSO (least absolute shrinkage and selection operator) machine-learning technique (Tibshirani, 1996), identified the combination of parameters that best correlated with their half-life and clearance values from the literature. The most important parameters were then used to predict the half-life and clearance of each mAb, revealing that just two biophysical determinants could be used to accurately predict human PK for this set of mAbs. Crucially, this empirical approach to the problem allows us to identify predictive parameters in an unbiased fashion and highlights correlations that could guide future mechanistic studies. Predictions could be further improved by refining this approach, perhaps by incorporating and testing some of the many other parameters that have been proposed to affect mAb PK.

Materials and Methods

Proteins. Clinical mAbs were obtained through clinical vendors by S.H.T. Size-exclusion chromatography and SDS-PAGE were performed to ensure the integrity of mAbs. Human FcRn with β_2-microglobulin (catalog #CT009-H08H-50) was purchased from Sino Biological (Wayne, PA). The presence of both the FcRn α-chain and β_2-microglobulin was verified by SDS-PAGE.

Biolayer Interferometry. Kinetic experiments were performed at 25°C on an Octet RED384 (ForteBio, Fremont, CA) using 96-well half-area plates at 1000 rpm and a total 100 μl/well. First, 2.5 μg/ml His-tagged human FcRn in 1× phosphate-buffered saline (PBS), pH 7.2 (8.10 mM Na_2HPO_4, 1.47 mM KH_2PO_4, 137 mM NaCl, 2.67 mM KCl) was loaded onto Ni-NTA sensor tips for 300 seconds to obtain a response of 2 nm. Two baseline steps were performed for 120 seconds and then 60 seconds by blocking with 1× PBS containing 1% casein (w/v) and 0.05% Tween 20 (v/v) brought to pH 6.0 or pH 7.0 using HCl. A 180-second association phase was performed with 66.7, 16.7, 4.17, and 1.04 nM IgG at pH 6.0 or 6670, 1670, 417, and 104 nM IgG at pH 7.0 (same buffer as in baseline steps). Dissociation was performed for 180 seconds in fresh buffer matching the baseline/association buffer.

Analysis was performed in Octet Data Analysis software version 7. Reference data (mAb binding to tips lacking FcRn) were subtracted from sample data. Association and dissociation data for a given mAb at pH 6.0 were globally fit using the 1:1 model with a linked maximal response (R_{max}) for the four concentrations. For pH 7.0 data, none of the models produced adequate global fits, so the response at the highest IgG concentration (6.67 μM) was used as a model-independent measure of pH 7.0 binding.

Differential Scanning Calorimetry. Thermal unfolding experiments were performed on a MicroCal VP-Capillary differential scanning calorimetry (DSC) (Malvern Panalytical, Malvern, UK) using 0.15 or 0.5 mg/ml IgG in 1× PBS, pH 7.2. IgG samples and reference buffer were scanned from 40 to 100°C at 60°C/h. Three buffer/buffer scans were run between each sample/buffer scan. After subtracting the buffer/buffer scan immediately preceding the sample/buffer scan and normalizing concentration, "Progress Baseline" subtraction was performed to obtain a thermogram with a flat baseline using Origin 7 software. Thermodynamic parameters melting temperature (T_m) and change in enthalpy of unfolding (ΔH) were obtained by fitting to a non–two-state model containing three peaks. The total ΔH was calculated as the sum of individual ΔH values. The weight-averaged T_m was obtained using the T_m and ΔH from each peak according to the following equation:

$$T_{m,avg} = \frac{\sum_{i=1}^{3} T_{m,i} \cdot \Delta H_i}{\sum_{i=1}^{3} \Delta H_i}$$

The change in heat capacity upon unfolding (ΔC_P) was determined by using the "Step at Half Area" baseline option and calculating the difference between baselines before and after the step. Using the "Step at Peak" option yielded essentially identical ΔC_P values ($R^2 = 0.998$). DSC parameters presented are the average of two independent experiments (one at 0.15 mg/ml and one at 0.5 mg/ml).

Regression Analysis. Literature reports of half-life and clearance were found by searching for a given antibody and "half-life" in PubMed (https://www.ncbi.nlm.nih.gov/pubmed) and selected based on a description of human clinical studies. FDA package inserts were used as additional references. Volumes of distribution at steady state for the various mAbs ranged within 2-fold (0.060–0.106 l/kg). All the studies either explicitly reported linear PK or did not specifically mention nonlinearity. When multiple doses or routes of administration were investigated, the average PK value of all conditions was used.

Analysis was performed in MATLAB (MathWorks, Natick, MA) R2017b using the "regress" and "lasso" functions. Prior to regression analysis, the six parameters [FcRn kinetic association rate constant (k_a) at pH 6.0, FcRn kinetic association rate constant (k_d) at pH 6.0, FcRn response at pH 7.0, ΔH, T_m, and ΔC_P] were tabulated with each column as a predictor and each row as a mAb. Parameters were normalized by subtracting the mean of the column and dividing by the S.D. of the column. Thus, the normalized columns all had a mean of 0 and an S.D. of 1, but retained their distribution of values for the different mAbs, ensuring that each parameter contributed equally to regression calculations. In linear regression, coefficients for each parameter are optimized so as to minimize the root mean square difference (RMSD) between observed and predicted values of a dependent variable (here, either half-life or clearance). LASSO involves a similar optimization, with the additional constraint that the sum of all the coefficients must be lower than a regularization parameter λ (Tibshirani, 1996). Higher values of λ favor simpler models with fewer nonzero coefficients, allowing us to rigorously explore the trade-off between model accuracy and model complexity.

After LASSO regression, models based on the optimal parameter pairs were calculated using the following equation:

$$y = m_1 \cdot x_1 + m_2 \cdot x_2 + b$$

where y is the two-parameter score, x_1 and x_2 are the parameter values (e.g., FcRn-IgG response at pH 7.0 and ΔC_P), m_1 and m_2 are the best-fit regression coefficients, and b is the regression intercept. For leave-one-out analysis, the half-life of each mAb in turn was predicted by performing a regression with the other seven mAbs, and then using the resulting intercept and coefficients along with the parameter values of the mAb to calculate its two-parameter score.

Results

To determine the relation between biophysical parameters of therapeutic mAbs and their PK characteristics, a small selection of mAbs with existing human half-life data were required. Eight clinical IgG1κ mAbs targeting soluble antigens were selected based on FDA package inserts and clinical trials describing half-lives ranging from 7.2 to 24.5 days (Table 1). These half-life values, and separately the mAb clearance values, were used as the dependent variables to which the independent variables (biophysical parameters) would be correlated.

Since FcRn is known to salvage IgG from lysosomal degradation and thus affect serum stability, the affinity of these eight mAbs for FcRn was examined as one potential determinant of half-life and clearance. In

particular, both the k_a and k_d values of the interaction at endosomal pH (pH 6.0) were determined by biolayer interferometry (BLI) because both kinetic parameters could be important predictors. The kinetic data fit well to the simplest 1:1 binding model, from which k_a and k_d parameters were extracted for each mAb (Fig. 1A; Supplemental Fig. 1; Table 1). When the IgG-FcRn k_a and k_d were compared with half-life and clearance, they unexpectedly revealed very weak correlations (Fig. 3, A and B). This suggests that FcRn affinity at endosomal pH is not the most important determinant of half-life and clearance for IgG1 mAbs containing different variable regions.

IgG-FcRn binding is highly pH dependent, with tight binding occurring only below pH ~6.5. For the FcRn salvage mechanism to be effective, an IgG must associate tightly with FcRn in the endosome; however, it also must be efficiently released from FcRn upon exposure to the neutral pH (pH 7.4) of the blood. Thus, the binding kinetics of the mAbs to FcRn at neutral pH were considered as another possible determinant of serum half-life, as previously considered by others (Wang et al., 2011; Borrok et al., 2015). Well-defined binding was not observed at pH 7.4, even with $>$ 1 mg/ml IgG binding to immobilized FcRn. Instead, binding and dissociation were examined at pH 7.0, which was the highest pH with quantifiable binding. The pH 7.0 data did not fit well with any simple models such as 1:1 or bivalent analyte, preventing the determination of accurate k_a and k_d values. This complexity may result from avidity in IgG-FcRn interactions (Abdiche et al., 2015). As an alternative, the maximum response achieved was tabulated as an objective, model-independent measure of binding at pH 7.0 (Fig. 1B; Supplemental Fig. 2; Table 1). Comparison of these response values with mAb half-lives revealed an inverse correlation, indicating that long mAb half-life is associated with weak FcRn binding at neutral pH (Fig. 3C). Conversely, FcRn response at pH 7.0 was positively correlated to clearance. Independent experiments confirmed the observed trends in FcRn binding at pH 6.0 and 7.0 (Supplemental Figs. 3–5).

Thermal stability, which varies based on the amino acid sequence, is another biophysical property of mAbs that may affect half-life. DSC was used to monitor unfolding as a function of temperature. Since IgG unfolding thermograms have been shown to be similar at endosomal and neutral pH, the experiments were performed only at pH 7.2 (Majumdar et al., 2015). After subtracting buffer scans and normalizing by concentration, the DSC data were fit to a non–two-state-state model with three components, which was the smallest number of components that accurately described each of the mAbs (Fig. 2A; Supplemental Figs. 6 and 7). From these fits, the total ΔH (sum of the ΔH values for each component) was tabulated, and revealed a weak negative correlation with half-life and a weak positive correlation with clearance (Fig. 3D; Table 1). The weight-averaged T_m was also calculated as the T_m of each fit component multiplied by the contribution of that component to the total ΔH. This T_m parameter showed a weak positive correlation with half-life and a weak negative correlation with clearance (Fig. 3E; Table 1). As a final predictor of half-life from DSC data, the difference in heat capacity between folded and unfolded states (ΔC_P) was calculated for each mAb. ΔC_P was inversely correlated with half-life and positively correlated with clearance (Fig. 2B; Fig. 3F; Supplemental Fig. 8; Table 1).

Comparing individual BLI or DSC parameters yielded generally weak correlations with half-life and clearance with $R^2 < 0.8$. Multiple regression was performed with all six parameters and yielded very

TABLE 1

Literature PKs and biophysical parameters for clinical mAbs

Antibody	Human Half-Life	Human Clearance	FcRn k_a, pH 6.0	FcRn k_d, pH 6.0	FcRn Response, pH 7.0	ΔH	Weight Average T_m	ΔC_P
	d	ml/day per kilogram	$mM^{-1}s^{-1}$	ks^{-1}	nm	kcal/mol	°C	kcal/mol per degree celsius
Adalimumab[a–c]	14.5 ± 2.7	4.2 ± 0.9	641 ± 1	1.59 ± 0.01	1.77	948 ± 1	73.9 ± 0.1	11.9 ± 1.1
Bevacizumab[d–g]	19.7 ± 0.4	3.0 ± 0.3	349 ± 0	0.96 ± 0.00	1.89	709 ± 69	72.6 ± 0.2	6.7 ± 2.3
Carlumab[h,i]	7.2 ± 0.4	13.2	437 ± 1	3.09 ± 0.01	1.97	884 ± 133	71.8 ± 0.2	21.1 ± 3.7
Golimumab[j–o]	12.4 ± 1.1	10.9 ± 4.0	459 ± 1	1.56 ± 0.00	2.05	854 ± 98	75.0 ± 0.1	18.3 ± 2.5
Infliximab[p–t]	12.1 ± 4.0	5.1 ± 0.7	423 ± 0	0.91 ± 0.00	1.96	843 ± 26	71.2 ± 0.1	12.4 ± 1.7
Omalizumab[u,v]	24.5 ± 2.1	2.4 ± 0.1	371 ± 0	1.64 ± 0.00	0.72	932 ± 55	78.5 ± 0.2	13.6 ± 2.2
Siltuximab[w,x]	19.9 ± 1.0	3.8 ± 0.7	505 ± 1	2.27 ± 0.01	1.10	706 ± 11	71.5 ± 0.1	13.5 ± 0.6
Ustekinumab[y,z]	24.2 ± 3.3	2.9	535 ± 1	2.38 ± 0.01	1.10	738 ± 45	73.1 ± 0.4	11.6 ± 3.9

[a]https://www.accessdata.fda.gov/drugsatfda_docs/label/2017/125057s399lbl.pdf.
[b]Weisman et al. (2003).
[c]den Broeder et al. (2002).
[d]https://www.accessdata.fda.gov/drugsatfda_docs/label/2016/125085s317lbl.pdf.
[e]Han et al. (2016).
[f]Li et al. (2013).
[g]Lu et al. (2008).
[h]https://ncats.nih.gov/files/CNTO-888.pdf.
[i]Sandhu et al. (2013).
[j]https://www.accessdata.fda.gov/drugsatfda_docs/label/2015/125433s014lbl.pdf.
[k]Zhuang et al. (2012).
[l]Zhuang et al. (2013).
[m]Ling et al. (2010).
[n]Xu et al. (2010).
[o]Zhou et al. (2007).
[p]https://www.accessdata.fda.gov/drugsatfda_docs/label/2013/103772s5359lbl.pdf.
[q]Dotan et al. (2014).
[r]Fasanmade et al. (2011).
[s]Cornillie et al. (2001).
[t]Ternant et al., 2008.
[u]https://www.accessdata.fda.gov/drugsatfda_docs/label/2016/103976s5225lbl.pdf.
[v]Hayashi et al. (2007).
[w]https://www.accessdata.fda.gov/drugsatfda_docs/label/2014/125496s000lbl.pdf.
[x]Kurzrock et al. (2013).
[y]https://www.accessdata.fda.gov/drugsatfda_docs/label/2016/761044lbl.pdf.
[z]Zhu et al. (2013).

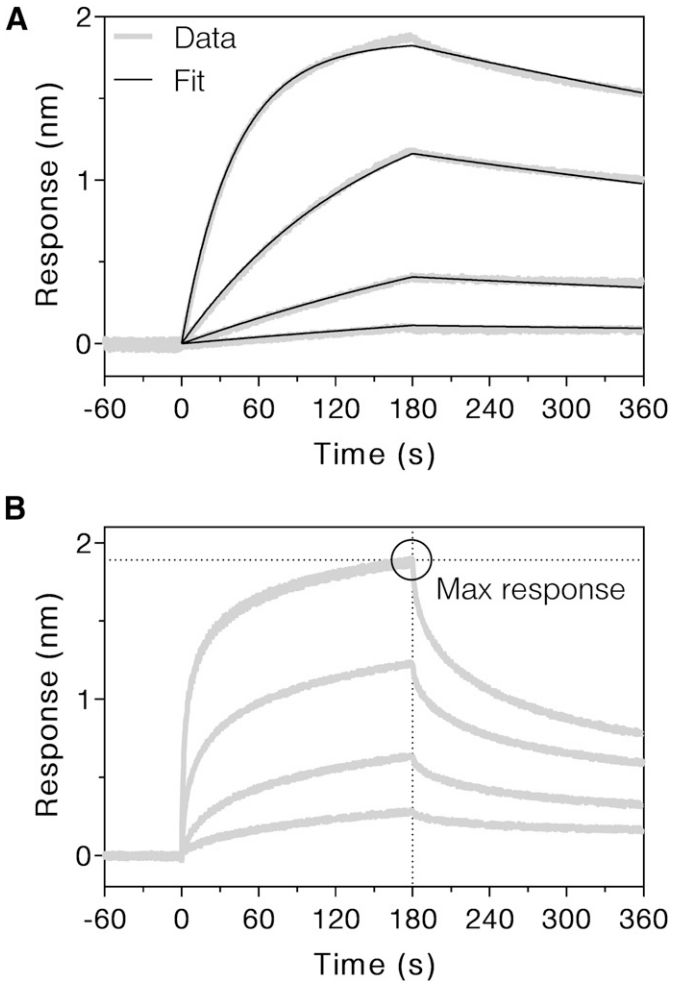

Fig. 1. BLI sensorgrams of bevacizumab binding to immobilized human FcRn at pH 6.0 (A) and 7.0 (B). At pH 6.0, Ni-NTA tips loaded with FcRn were dipped in buffer containing 66.7, 16.7, 4.17, or 1.04 nM bevacizumab to observe the association phase for 3 minutes, followed by dipping in buffer lacking bevacizumab to observe the dissociation phase for 3 minutes. Thick gray lines show the data, and narrow black lines show a global fit of all four concentrations to a 1:1 binding model, which yielded kinetic parameters k_a and k_d. At pH 7.0, Ni-NTA tips loaded with FcRn were dipped in buffer containing 6670, 1670, 417, or 104 nM bevacizumab to observe the association phase for 3 minutes, followed by dipping in buffer lacking bevacizumab to observe the dissociation phase for 3 minutes. Thick gray lines show the data, and the black circle highlights the maximum binding response achieved for the 6.67 μM concentration. FcRn binding data at pH 6.0 and 7.0 are shown for other mAbs in Supplemental Figs. 1–5. Max, maximum.

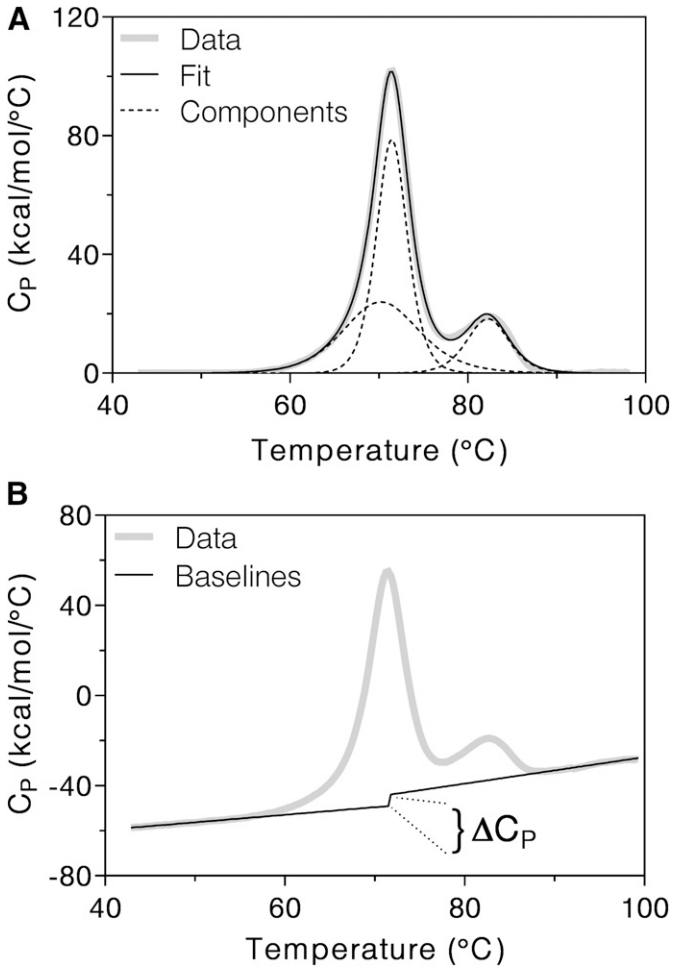

Fig. 2. DSC thermograms showing the unfolding of bevacizumab at pH 7.2. (A) After performing "Progress Baseline" subtraction, the data were fit to a three-component, non–two-state model to extract the ΔH and T_m associated with three unfolding events. Data are shown as a thick gray line, the fit is shown as a narrow black line, and the fitted components are shown as black dotted lines. (B) Baselines of the folded and unfolded states were fit using the "Step at Half Area" baseline option. The difference in C_P at half area was calculated as the ΔC_P. Replicates, peak fits, and baseline fits are shown for all mAbs in Supplemental Figs. 6–8.

strong correlations with $R^2 = 0.99$, but, as expected, the data were severely undersampled and overfit, resulting in large S.E. values in parameter coefficients. To determine which subset of coefficients would yield the best correlation with half-life and clearance, LASSO regression was applied to reduce the number of predictors by introducing the regularization parameter λ (Tibshirani, 1996, 2011). Applying LASSO to the tabulated mAb parameters revealed different solutions to the regression problem depending on the value of λ. As the value of λ was increased, the number of nonzero coefficients decreased while the mean squared error increased (Fig. 4). Based on this analysis, the best single parameter for half-life prediction was FcRn response at pH 7.0 (consistent with the high R^2 value for this individual correlation). Examining solutions for lower values of λ revealed that the combination of two parameters most strongly associated with half-life was FcRn response at pH 7.0 and ΔC_P. These same two parameters were also the best combination of clearance determinants, though in the opposite order of importance. To ensure that this analysis was not discounting the pH 6.0 binding data because it was represented by two distinct parameters, LASSO regression was also performed using the maximum response at pH 6.0 instead of both k_a and k_d. This five-parameter regression yielded results similar to those of the original six-parameter solution: response at pH 7.0 and ΔC_P remained the top pair of predictors for both half-life and clearance (Supplemental Fig. 9).

Next, normal multiple regression was performed using FcRn response at pH 7.0 and ΔC_P as the only two predictors for half-life. This was done to determine best-fit coefficients for the parameters without applying any penalty function for the number of parameters. The resulting correlation between the linear combination of these two parameters and half-life or clearance was much stronger than the correlation for each individual parameter ($R^2 = 0.91$ and $R^2 = 0.96$, respectively, Fig. 5, A and B). Because the parameter matrix was normalized to have a mean of 0 and an S.D. of 1 prior to analysis, any differences in the magnitude or range of parameters were eliminated. In other words, regression results will depend on relative differences rather than on absolute values of biophysical parameters. Thus, the regression coefficients reflect the

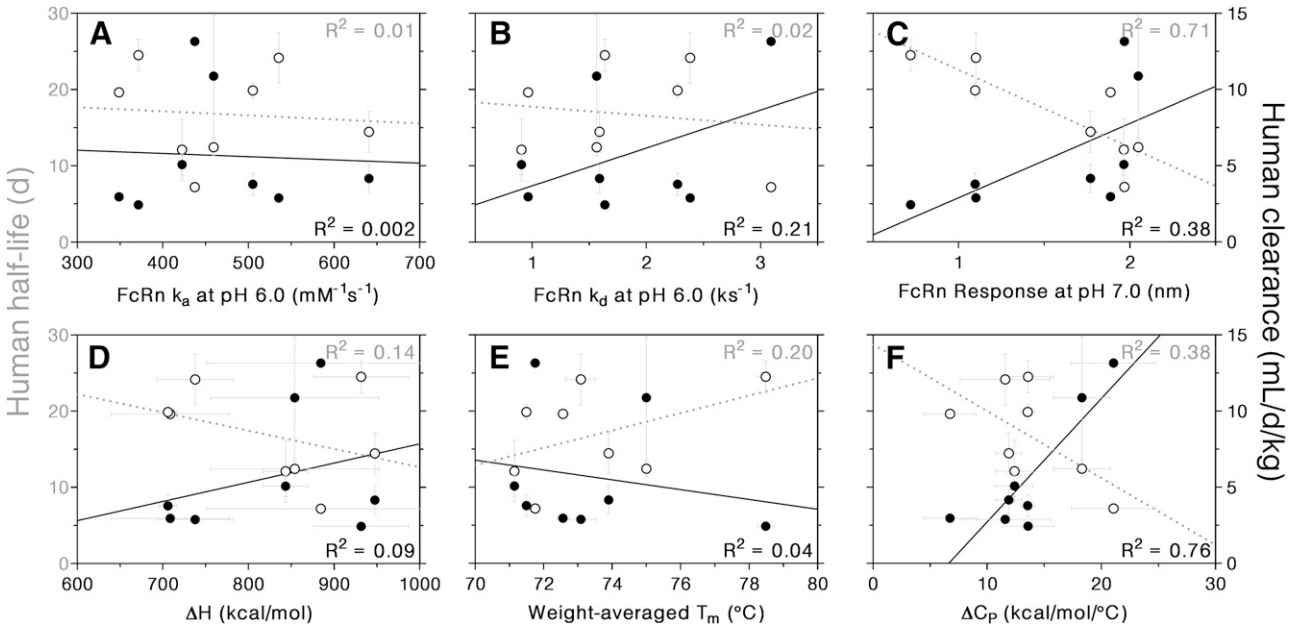

Fig. 3. Correlations between mAb half-life or clearance and individual biophysical parameters. The FcRn k_a values at pH 6.0 (A), FcRn k_d values at pH 6.0 (B), and FcRn maximum binding response after 3 minutes at pH 7.0 (C) were obtained from BLI experiments. The values for total ΔH (D), weight-averaged T_m (E), and ΔC_P of unfolding (F) were obtained from DSC experiments. Half-life values are plotted on the left axis as open circles, with linear fits plotted as gray dotted lines containing the gray R^2 values listed at the top right. Clearance values are plotted on the right axis as closed circles, with linear fits plotted as black solid lines containing the black R^2 values listed at the bottom right.

relative importance of each parameter for half-life or clearance prediction. In this case, the half-life coefficient for pH 7.0 response was -4.63 ± 0.83, and for ΔC_P was -2.88 ± 0.83 with an intercept of 16.8 ± 0.8. In other words, both pH 7.0 response and ΔC_P were negatively correlated with half-life, but pH 7.0 response was somewhat more important for the two-parameter correlation. For clearance, ΔC_P was the more important of the two determinants. The pH 7.0 response coefficient was 1.86 ± 0.35, the ΔC_P coefficient was 3.15 ± 0.35, and the intercept was 5.67 ± 0.32.

To test the robustness of the two-parameter correlation and assess its predictive power, we performed leave-one-out (also called "jackknife") subsampling: the half-life and clearance of each mAb were predicted based on the measured biophysical parameters of the mAb and a regression model trained on the other seven mAbs. When LASSO analysis was performed for each subset of mAbs, all but one subset yielded pH 7.0 response and ΔC_P as the primary two determinants for both half-life and clearance. When omalizumab was excluded, these two parameters were most important for clearance; but for half-life, pH 7.0 response, ΔH, and ΔC_P were the first three determinants. Despite this single exception, for consistency, the pH 7.0 response and ΔC_P of each mAb were used to predict its half-life and clearance. The values of the regression intercept and coefficients were similar when any one of the mAbs was omitted from the correlations (Table 2). Indeed, the S.D. for the intercept, the pH 7.0 response coefficient, and the ΔC_P coefficient from subsampling analysis were all under 16% for both half-life and clearance.

The prediction of mAb half-life based on its pH 7.0 response and ΔC_P was fairly accurate, with differences between measured and predicted half-lives ranging from 0 to 4.7 days (0%–38%) and a RMSD of 2.7 days (16%). Comparing the leave-one-out two-parameter predicted half-life of an mAb to the reported value resulted in a correlation of $R^2 = 0.79$ (Fig. 5C). Analogous prediction of mAb clearance based on the same two parameters resulted in an RMSD of 1.4 ml/day per kilogram (24%). In this case, the correlation between predicted and reported clearance indicated strong predictive power ($R^2 = 0.88$) (Fig. 5D).

Discussion

The half-life of a therapeutic mAb is a vital biologic characteristic that determines how frequently the drug must be administered. In many cases, it is desirable to invest in mAbs that have slow elimination kinetics, so they can be administered at a lower dose or reduced frequency, ultimately saving time and money for both patients and companies. Despite the incentive for characterizing mAb half-life early in the drug pipeline, it has been difficult to predict the PK properties of mAbs before they enter human trials. Many individual parameters, including biologic properties like FcRn affinity or glycosylation state, biophysical properties like nonspecific binding or aggregation propensity, and sequence-based properties like allotype, have been correlated to half-life with varying degrees of interdependence (Wang et al., 2011; Datta-Mannan et al., 2015a; Ternant et al., 2016; Tibbitts et al., 2016). It appears that no single property of an mAb can be used to accurately predict PK properties. At the same time, it would be advantageous to know the smallest, most tractable set of parameters that would be predictively useful. Thus, we took a combinatorial approach to determine whether half-life prediction could be improved using multiple parameters incorporated into a cohesive model. The LASSO machine-learning approach provides a statistically rigorous method to identify parameter combinations that best predict outcomes.

In forming a panel of mAbs to analyze, various factors were considered. The primary goal was to obtain a small sample of mAbs with a large spread of human half-life values based on published clinical data. Thus, mAbs were selected with half-lives ranging from 1 week to over 3 weeks. Because the subtype of IgG heavy chain is known to affect mAb PK, with IgG3 having a shorter serum half-life than other subtypes, only IgG1 mAbs were considered for analysis

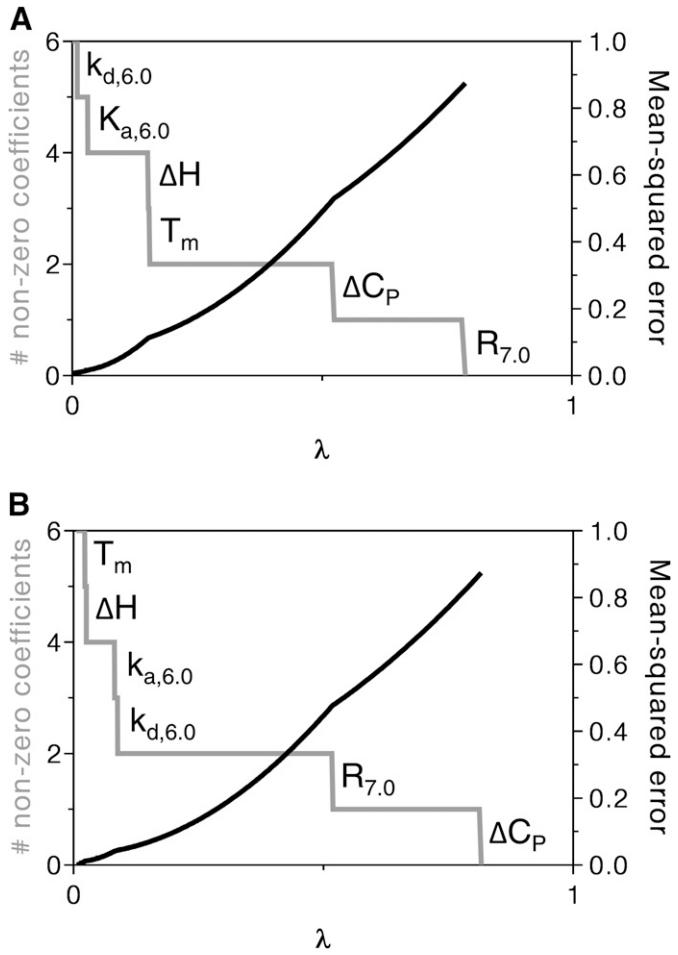

Fig. 4. LASSO analysis to determine the most important predictors of mAb half-life (A) and clearance (B). As the value of the regularization parameter λ increased, the number of nonzero coefficients (gray line, left axis) decreased while the mean squared error (black line, right axis) increased. The most important parameters for multiple regression of half-life (introduced at the highest values of λ) were pH 7.0 response ($R_{7.0}$), ΔC_P of unfolding, weight-averaged T_m, total ΔH of unfolding, pH 6.0 k_a ($k_{a,6.0}$), and pH 6.0 k_d ($k_{d,6.0}$), in that order. For clearance, the order of importance was ΔC_P, $R_{7.0}$, $k_{d,6.0}$, $k_{a,6.0}$, ΔH, and T_m.

(Stapleton et al., 2011). Likewise, all the selected mAbs contained κ-light chains. Only mAbs that target soluble antigens were selected, to minimize differences in half-life that occur as a result of receptor-mediated disposition or other target-dependent processes and to emphasize intrinsic biophysical parameters. Of course, it was not possible to eliminate every source of variation with the relatively small number of mAbs available to us. The panel contains mAbs that are chimeric, humanized, or fully human, and allotypes m3,1; m17,1; and m17,−1 are all represented. However, neither framework nor allotype were associated with significant differences in half-life or clearance (Supplemental Fig. 10).

The FcRn binding data at pH 6.0 yielded higher affinities than some reports in the literature, due to the level of FcRn immobilized and the bivalent mechanism of FcRn-IgG binding (Suzuki et al., 2010; Wang et al., 2011). Nevertheless, the data within this experiment are directly comparable and revealed modest differences in association and dissociation rates that were not correlated with half-life. As the FcRn binding interface of these mAbs is identical, it is possible that the observed differences in FcRn binding are caused by charge-mediated Fab-FcRn interactions (Schoch et al., 2015). Previous studies have noted that stronger FcRn binding at endosomal pH leads to enhanced IgG half-life (Dall'Acqua et al., 2006; Hinton et al., 2006; Zalevsky et al., 2010). It should be noted that these studies compare the clearance of a given mAb with and without mutations that affect FcRn binding. The variable regions of the mAb are conserved, and the biophysical properties of the mutants are expected to be similar. Localization of mutations to the FcRn binding site creates large (10- to 30-fold) increases in FcRn affinity that are much larger than the 3-fold span in affinity observed here. In these cases, it makes sense that FcRn binding would be a primary determinant of half-life. Other studies have shown that FcRn binding at pH 6 is not strongly associated with half-life when distinct clinical mAbs are examined, or even when the variable regions are maintained (Dall'Acqua et al., 2002; Gurbaxani et al., 2006; Wang et al., 2011; Datta-Mannan et al., 2012).

The ability of mAbs to bind FcRn at pH 7.0, however, was strikingly related to their half-lives in humans. Although it was not possible to reliably extract k_a and k_d values at pH 7, the maximum response achieved at the highest mAb concentration provided an objective measure of binding that was negatively correlated with half-life. As the mass and concentration of mAbs were effectively equal and the association times were identical, the response parameter provides an unbiased measure of FcRn binding. The inverse correlation between neutral pH binding and half-life has been observed previously by groups showing that weak FcRn binding at neutral pH is just as important as tight binding in the endosome (Wang et al., 2011; Borrok et al., 2015). The observation that excessive binding at neutral pH accelerates clearance may be due to FcRn-dependent endocytosis and degradation or FcRn-independent processes related to nonspecific binding. The inability to globally fit the pH 7 data, although inconvenient, may suggest the presence of multiple conformations or protonation states of the Fc or FcRn at this pH, or of polyvalent interactions, which complicates simple 1:1 fits.

It is reasonable that the serum stability of an mAb would be related to its inherent thermal stability. Molecules containing unstable variable regions may be more prone to unfold or aggregate. Both processes would be expected to accelerate clearance, either due to the generation of an immune response or the loss of FcRn binding capacity (Ratanji et al., 2014; Roberts, 2014). This hypothesis is supported by DSC data showing a weak but positive correlation between weight-averaged T_m and half-life. Interestingly, the correlation for ΔC_P and half-life was negative, suggesting that mAbs containing more buried hydrophobic residues are more likely to have shorter half-lives. Indeed, ΔC_P was moderately positively correlated with the grand average of hydropathy (GRAVY) score ($R^2 = 0.33$) (Supplemental Fig. 11) based on the amino acid sequence of the mAb variable regions (Kyte and Doolittle, 1982). An abundance of buried hydrophobic residues can stabilize the folded state in buffer, but may introduce opportunities for aggregation and other nonspecific interactions in the presence of other proteins or tissue constituents. Thus, the biologic matrix could actually destabilize the monomeric folded state if nonspecific, hydrophobically driven interactions pull the equilibrium toward unfolding or aggregation with serum components. Although previous efforts have examined less direct measures of stability such as nonspecific binding or self-association (Avery et al., 2018), our use of DSC enables the delineation of the precise thermodynamic parameters that provide the most predictive value.

A challenge associated with half-life prediction is how to account for the effects of multiple determinants without overparameterizing the model. Here, LASSO was used to identify the most powerful combination of two biophysical parameters for half-life and clearance prediction. The advantage of using LASSO was the ability to explore all possible combinations of parameters and to vary the value of λ so

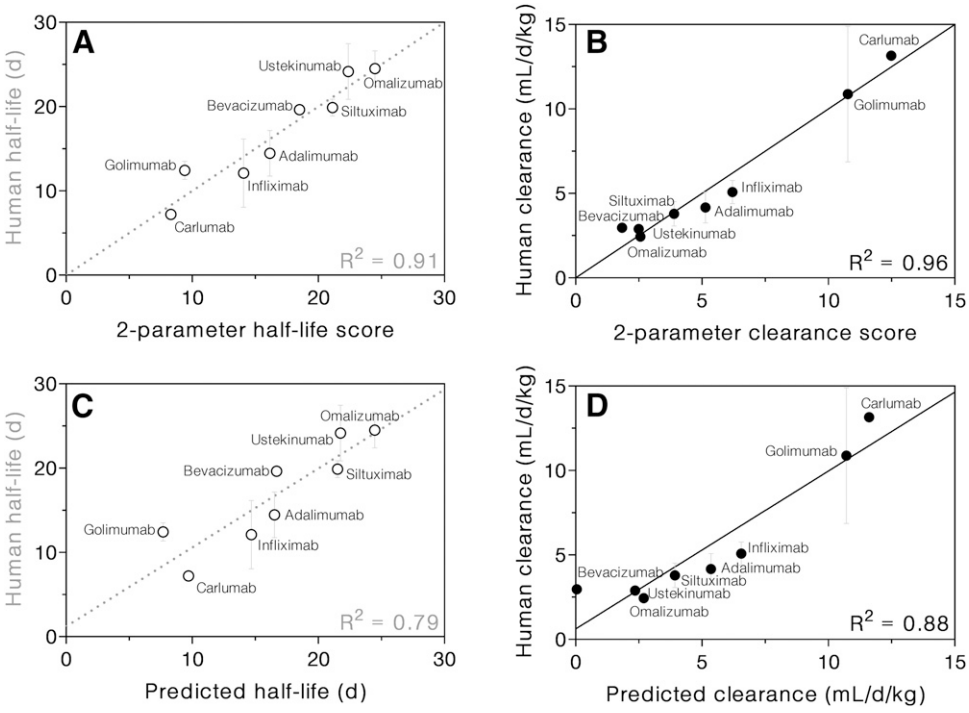

Fig. 5. mAb half-life (A) and clearance (B) correlated strongly with the respective two-parameter scores, which are based on the FcRn response at pH 7.0 and ΔC_P. Half-life (C) and clearance (D) predictions were validated using leave-one-out analysis. Multiple regression was performed using response at pH 7.0 and ΔC_P as predictors. Each mAb in turn was omitted from the regression, and then its values of pH 7 response and ΔC_P were used to predict its half-life or clearance using the regression results of the remaining seven mAbs.

that the number of nonzero coefficients ranged from 0 to 6. In this way, the response at pH 7.0 and the ΔC_P were identified as the two parameters that, in combination, yielded the best correlation to both half-life and clearance. Thus, accounting for both FcRn binding at neutral pH and thermodynamic stability allows for the most accurate prediction of mAb PK.

The approach taken here was fundamentally empirical in nature and designed more to generate hypotheses than to test them. Experiments were devised to allow for the extraction of biophysical parameters that may be associated with mAb serum stability. Although the limited set of predictors selected for analysis was guided by current knowledge of mAb PK, the analysis was not biased by our current mechanistic understanding of mAb recycling and clearance. This approach is therefore useful for generating new hypotheses about the phenomenon of interest. In this case, analysis identified pH 7 response and ΔC_P as predictors that are inversely correlated with half-life and positively correlated with clearance. Although the importance of FcRn release at neutral pH has been demonstrated, we did not encounter any previous reports that low ΔC_P values contribute to long mAb half-life. Perhaps the relationship between ΔC_P and clearance can be further explored to clarify the mechanism behind this observation.

Importantly, the parameters we considered by no means encompass all the factors that could affect the disposition of a particular mAb. A number of additional biophysical properties, reflective of protein stability, nonspecific binding, and aggregation propensity, have been advanced as important predictive metrics of PK and pharmacodynamics (Tibbitts et al., 2016; Jain et al., 2017). Expanding the use of LASSO and similar regression analyses to larger datasets, covering more samples and including more biophysical parameters, could prove informative, particularly in clarifying which in vitro parameters should be emphasized. Empirical, combinatorial approaches such as the one developed here could be generally useful for many different mAb-based therapeutics or for non-mAb therapeutics whose PK can be predicted by other combinations of biophysical determinants.

TABLE 2

Prediction of mAb half-life and clearance using leave-one-out regression

Antibody Omitted and Predicted	Half-Life Prediction			Clearance Prediction		
	Intercept	FcRn Response, pH 7.0 Coefficient	ΔC_P Coefficient	Intercept	FcRn Response, pH 7.0 Coefficient	ΔC_P Coefficient
Adalimumab	17.1 ± 0.8	−4.48 ± 0.87	−3.03 ± 0.87	5.82 ± 0.33	1.94 ± 0.34	3.07 ± 0.34
Bevacizumab	16.4 ± 0.9	−5.04 ± 0.99	−2.13 ± 1.25	5.31 ± 0.19	1.45 ± 0.20	3.90 ± 0.26
Carlumab	17.1 ± 0.9	−4.47 ± 0.90	−2.31 ± 1.17	5.48 ± 0.35	1.76 ± 0.35	2.80 ± 0.46
Golimumab	16.2 ± 0.6	−5.13 ± 0.60	−3.50 ± 0.62	5.65 ± 0.39	1.84 ± 0.41	3.13 ± 0.43
Infliximab	17.1 ± 0.8	−4.31 ± 0.87	−3.05 ± 0.83	5.86 ± 0.30	2.04 ± 0.32	3.06 ± 0.31
Omalizumab	16.8 ± 1.0	−4.62 ± 1.26	−2.89 ± 0.94	5.71 ± 0.40	1.80 ± 0.53	3.17 ± 0.40
Siltuximab	17.0 ± 0.9	−4.85 ± 0.96	−2.84 ± 0.89	5.69 ± 0.39	1.84 ± 0.42	3.16 ± 0.39
Ustekinumab	16.5 ± 0.8	−4.34 ± 0.89	−2.78 ± 0.84	5.61 ± 0.38	1.93 ± 0.41	3.18 ± 0.38
Average	16.8 ± 0.4	−4.66 ± 0.32	−2.82 ± 0.43	5.64 ± 0.18	1.83 ± 0.18	3.18 ± 0.31
(None omitted)	16.8 ± 0.8	−4.63 ± 0.83	−2.88 ± 0.83	5.67 ± 0.32	1.86 ± 0.35	3.15 ± 0.35

Acknowledgments

DSC experiments were performed at the Analytical Biopharmacy Core facility of the University of Washington. We thank John Sumida for assistance with DSC instrumentation and software.

Authorship Contributions

Participated in research design: Goulet, Tam, Chiu, Atkins, and Nath.

Conducted experiments: Goulet and Watson.

Contributed new reagents or analytic tools: Tam and Zwolak.

Performed data analysis: Goulet.

Wrote or contributed to the writing of the manuscript: Goulet, Watson, Tam, Zwolak, Chiu, Atkins, and Nath.

References

Abdiche YN, Yeung YA, Chaparro-Riggers J, Barman I, Strop P, Chin SM, Pham A, Bolton G, McDonough D, Lindquist K, et al. (2015) The neonatal Fc receptor (FcRn) binds independently to both sites of the IgG homodimer with identical affinity. *MAbs* **7**:331–343.

Avery LB, Wade J, Wang M, Tam A, King A, Piche-Nicholas N, Kavosi MS, Penn S, Cirelli D, Kurz JC, et al. (2018) Establishing *in vitro in vivo* correlations to screen monoclonal antibodies for physicochemical properties related to favorable human pharmacokinetics. *MAbs* **10**:244–255.

Beck A, Goetsch L, Dumontet C, and Corvaïa N (2017) Strategies and challenges for the next generation of antibody-drug conjugates. *Nat Rev Drug Discov* **16**:315–337.

Borrok MJ, Wu Y, Beyaz N, Yu X-Q, Oganesyan V, Dall'Acqua WF, and Tsui P (2015) pH-dependent binding engineering reveals an FcRn affinity threshold that governs IgG recycling. *J Biol Chem* **290**:4282–4290.

Cornillie F, Shealy D, D'Haens G, Geboes K, Van Assche G, Ceuppens J, Wagner C, Schaible T, Plevy SE, Targan SR, et al. (2001) Infliximab induces potent anti-inflammatory and local immunomodulatory activity but no systemic immune suppression in patients with Crohn's disease. *Aliment Pharmacol Ther* **15**:463–473.

Dall'Acqua WF, Kiener PA, and Wu H (2006) Properties of human IgG1s engineered for enhanced binding to the neonatal Fc receptor (FcRn). *J Biol Chem* **281**:23514–23524.

Dall'Acqua WF, Woods RM, Ward ES, Palaszynski SR, Patel NK, Brewah YA, Wu H, Kiener PA, and Langermann S (2002) Increasing the affinity of a human IgG1 for the neonatal Fc receptor: biological consequences. *J Immunol* **169**:5171–5180.

Datta-Mannan A, Chow CK, Dickinson C, Driver D, Lu J, Witcher DR, and Wroblewski VJ (2012) FcRn affinity-pharmacokinetic relationship of five human IgG4 antibodies engineered for improved in vitro FcRn binding properties in cynomolgus monkeys. *Drug Metab Dispos* **40**:1545–1555.

Datta-Mannan A, Lu J, Witcher DR, Leung D, Tang Y, and Wroblewski VJ (2015a) The interplay of non-specific binding, target-mediated clearance and FcRn interactions on the pharmacokinetics of humanized antibodies. *MAbs* **7**:1084–1093.

Datta-Mannan A, Thangaraju A, Leung D, Tang Y, Witcher DR, Lu J, and Wroblewski VJ (2015b) Balancing charge in the complementarity-determining regions of humanized mAbs without affecting pI reduces non-specific binding and improves the pharmacokinetics. *MAbs* **7**:483–493.

den Broeder A, van de Putte L, Rau R, Schattenkirchner M, Van Riel P, Sander O, Binder C, Fenner H, Bankmann Y, Velagapudi R, et al. (2002) A single dose, placebo controlled study of the fully human anti-tumor necrosis factor-alpha antibody adalimumab (D2E7) in patients with rheumatoid arthritis. *J Rheumatol* **29**:2288–2298.

Dostalek M, Prueksaritanont T, and Kelley RF (2017) Pharmacokinetic de-risking tools for selection of monoclonal antibody lead candidates. *MAbs* **9**:756–766.

Dotan I, Ron Y, Yanai H, Becker S, Fishman S, Yahav L, Ben Yehoyada M, and Mould DR (2014) Patient factors that increase infliximab clearance and shorten half-life in inflammatory bowel disease: a population pharmacokinetic study. *Inflamm Bowel Dis* **20**:2247–2259.

Fasanmade AA, Adedokun OJ, Blank M, Zhou H, and Davis HM (2011) Pharmacokinetic properties of infliximab in children and adults with Crohn's disease: a retrospective analysis of data from 2 phase III clinical trials. *Clin Ther* **33**:946–964.

Gurbaxani B, Dela Cruz LL, Chintalacharuvu K, and Morrison SL (2006) Analysis of a family of antibodies with different half-lives in mice fails to find a correlation between affinity for FcRn and serum half-life. *Mol Immunol* **43**:1462–1473.

Han K, Peyret T, Marchand M, Quartino A, Gosselin NH, Girish S, Allison DE, and Jin J (2016) Population pharmacokinetics of bevacizumab in cancer patients with external validation. *Cancer Chemother Pharmacol* **78**:341–351.

Hayashi N, Tsukamoto Y, Sallas WM, and Lowe PJ (2007) A mechanism-based binding model for the population pharmacokinetics and pharmacodynamics of omalizumab. *Br J Clin Pharmacol* **63**:548–561.

Hinton PR, Xiong JM, Johlfs MG, Tang MT, Keller S, and Tsurushita N (2006) An engineered human IgG1 antibody with longer serum half-life. *J Immunol* **176**:346–356.

Jain T, Sun T, Durand S, Hall A, Houston NR, Nett JH, Sharkey B, Bobrowicz B, Caffry I, Yu Y, et al. (2017) Biophysical properties of the clinical-stage antibody landscape. *Proc Natl Acad Sci USA* **114**:944–949.

Kaplon H and Reichert JM (2018) Antibodies to watch in 2018. *MAbs* **10**:183–203.

Kurzrock R, Voorhees PM, Casper C, Furman RR, Fayad L, Lonial S, Borghaei H, Jagannath S, Sokol L, Usmani SZ, et al. (2013) A phase I, open-label study of siltuximab, an anti-IL-6 monoclonal antibody, in patients with B-cell non-Hodgkin lymphoma, multiple myeloma, or Castleman disease. *Clin Cancer Res* **19**:3659–3670.

Kyte J and Doolittle RF (1982) A simple method for displaying the hydropathic character of a protein. *J Mol Biol* **157**:105–132.

Li J, Gupta M, Jin D, Xin Y, Visich J, and Allison DE (2013) Characterization of the long-term pharmacokinetics of bevacizumab following last dose in patients with resected stage II and III carcinoma of the colon. *Cancer Chemother Pharmacol* **71**:575–580.

Ling J, Lyn S, Xu Z, Achira M, Bouman-Thio E, Shishido A, Ford J, Shankar G, Wagner C, Kim KT, et al. (2010) Lack of racial differences in the pharmacokinetics of subcutaneous golimumab in healthy Japanese and Caucasian male subjects. *J Clin Pharmacol* **50**:792–802.

Lu J-F, Bruno R, Eppler S, Novotny W, Lum B, and Gaudreault J (2008) Clinical pharmacokinetics of bevacizumab in patients with solid tumors. *Cancer Chemother Pharmacol* **62**:779–786.

Majumdar R, Esfandiary R, Bishop SM, Samra HS, Middaugh CR, Volkin DB, and Weis DD (2015) Correlations between changes in conformational dynamics and physical stability in a mutant IgG1 mAb engineered for extended serum half-life. *MAbs* **7**:84–95.

Raghavan M, Bonagura VR, Morrison SL, and Bjorkman PJ (1995) Analysis of the pH dependence of the neonatal Fc receptor/immunoglobulin G interaction using antibody and receptor variants. *Biochemistry* **34**:14649–14657.

Ratanji KD, Derrick JP, Dearman RJ, and Kimber I (2014) Immunogenicity of therapeutic proteins: influence of aggregation. *J Immunotoxicol* **11**:99–109.

Robbie GJ, Criste R, Dall'acqua WF, Jensen K, Patel NK, Losonsky GA, and Griffin MP (2013) A novel investigational Fc-modified humanized monoclonal antibody, motavizumab-YTE, has an extended half-life in healthy adults. *Antimicrob Agents Chemother* **57**:6147–6153.

Roberts CJ (2014) Therapeutic protein aggregation: mechanisms, design, and control. *Trends Biotechnol* **32**:372–380.

Roopenian DC and Akilesh S (2007) FcRn: the neonatal Fc receptor comes of age. *Nat Rev Immunol* **7**:715–725.

Roopenian DC, Christianson GJ, Sproule TJ, Brown AC, Akilesh S, Jung N, Petkova S, Avanessian L, Choi EY, Shaffer DJ, et al. (2003) The MHC class I-like IgG receptor controls perinatal IgG transport, IgG homeostasis, and fate of IgG-Fc-coupled drugs. *J Immunol* **170**:3528–3533.

Sandhu SK, Papadopoulos K, Fong PC, Patnaik A, Messiou C, Olmos D, Wang G, Tromp BJ, Puchalski TA, Balkwill F, et al. (2013) A first-in-human, first-in-class, phase I study of carlumab (CNTO 888), a human monoclonal antibody against CC-chemokine ligand 2 in patients with solid tumors. *Cancer Chemother Pharmacol* **71**:1041–1050.

Schoch A, Kettenberger H, Mundigl O, Winter G, Engert J, Heinrich J, and Emrich T (2015) Charge-mediated influence of the antibody variable domain on FcRn-dependent pharmacokinetics. *Proc Natl Acad Sci USA* **112**:5997–6002.

Souders CA, Nelson SC, Wang Y, Crowley AR, Klempner MS, and Thomas W Jr (2015) A novel in vitro assay to predict neonatal Fc receptor-mediated human IgG half-life. *MAbs* **7**:912–921.

Spiess C, Zhai Q, and Carter PJ (2015) Alternative molecular formats and therapeutic applications for bispecific antibodies. *Mol Immunol* **67** (2 Pt A):95–106.

Stapleton NM, Andersen JT, Stemering AM, Bjarnarson SP, Verheul RC, Gerritsen J, Zhao Y, Kleijer M, Sandlie I, de Haas M, Jonsdottir I, van der Schoot CE, and Vidarsson G (2011) Competition for FcRn-mediated transport gives rise to short half-life of human IgG3 and offers therapeutic potential. *Nat Comm* **2** (599):1–9.

Suzuki T, Ishii-Watabe A, Tada M, Kobayashi T, Kanayasu-Toyoda T, Kawanishi T, and Yamaguchi T (2010) Importance of neonatal FcR in regulating the serum half-life of therapeutic proteins containing the Fc domain of human IgG1: a comparative study of the affinity of monoclonal antibodies and Fc-fusion proteins to human neonatal FcR. *J Immunol* **184**:1968–1976.

Tam SH, McCarthy SG, Brosnan K, Goldberg KM, and Scallon BJ (2013) Correlations between pharmacokinetics of IgG antibodies in primates vs. FcRn-transgenic mice reveal a rodent model with predictive capabilities. *MAbs* **5**:397–405.

Ternant D, Arnoult C, Pugnière M, Dhommée C, Drocourt D, Perouzel E, Passot C, Baroukh N, Mulleman D, Tiraby G, et al. (2016) IgG1 allotypes influence the pharmacokinetics of therapeutic monoclonal antibodies through FcRn binding. *J Immunol* **196**:607–613.

Ternant D, Aubourg A, Magdelaine-Beuzelin C, Degenne D, Watier H, Picon L, and Paintaud G (2008) Infliximab pharmacokinetics in inflammatory bowel disease patients. *Ther Drug Monit* **30**:523–529.

Tibshirani R (1996) Regression selection and shrinkage via the lasso. *J R Stat Soc B* **58**:267–288.

Tibshirani R (2011) Regression shrinkage and selection via the lasso: a retrospective. *J R Stat Soc B* **73**:273–282.

Tibbitts J, Canter D, Graff R, Smith A, and Khawli LA (2016) Key factors influencing ADME properties of therapeutic proteins: a need for ADME characterization in drug discovery and development. *MAbs* **8**:229–245.

Wang W, Lu P, Fang Y, Hamuro L, Pittman T, Carr B, Hochman J, and Prueksaritanont T (2011) Monoclonal antibodies with identical Fc sequences can bind to FcRn differentially with pharmacokinetic consequences. *Drug Metab Dispos* **39**:1469–1477.

Wang W, Wang EQ, and Balthasar JP (2008) Monoclonal antibody pharmacokinetics and pharmacodynamics. *Clin Pharmacol Ther* **84**:548–558.

Weisman MH, Moreland LW, Furst DE, Weinblatt ME, Keystone EC, Paulus HE, Teoh LS, Velagapudi RB, Noertersheuser PA, Granneman GR, et al. (2003) Efficacy, pharmacokinetic, and safety assessment of adalimumab, a fully human anti-tumor necrosis factor-alpha monoclonal antibody, in adults with rheumatoid arthritis receiving concomitant methotrexate: a pilot study. *Clin Ther* **25**:1700–1721.

Xu Z, Wang Q, Zhuang Y, Frederick B, Yan H, Bouman-Thio E, Marini JC, Keen M, Snead D, Davis HM, et al. (2010) Subcutaneous bioavailability of golimumab at 3 different injection sites in healthy subjects. *J Clin Pharmacol* **50**:276–284.

Zalevsky J, Chamberlain AK, Horton HM, Karki S, Leung IWL, Sproule TJ, Lazar GA, Roopenian DC, and Desjarlais JR (2010) Enhanced antibody half-life improves in vivo activity. *Nat Biotechnol* **28**:157–159.

Zhou H, Jang H, Fleischmann RM, Bouman-Thio E, Xu Z, Marini JC, Pendley C, Jiao Q, Shankar G, Marciniak SJ, et al. (2007) Pharmacokinetics and safety of golimumab, a fully human anti-TNF-α monoclonal antibody, in subjects with rheumatoid arthritis. *J Clin Pharmacol* **47**:383–396.

Zhu Y, Wang Q, Frederick B, Bouman-Thio E, Marini JC, Keen M, Petty KJ, Davis HM, and Zhou H (2013) Comparison of the pharmacokinetics of subcutaneous ustekinumab between Chinese and non-Chinese healthy male subjects across two phase 1 studies. *Clin Drug Investig* **33**:291–301.

Zhuang Y, Lyn S, Lv Y, Xu Z, Bouman-Thio E, Masterson T, Ford JA, Keen M, Petty KJ, Davis HM, et al. (2013) Pharmacokinetics and safety of golimumab in healthy Chinese subjects following a single subcutaneous administration in a randomized phase I trial. *Clin Drug Investig* **33**:795–800.

Zhuang Y, Xu Z, Frederick B, de Vries DE, Ford JA, Keen M, Doyle MK, Petty KJ, Davis HM, and Zhou H (2012) Golimumab pharmacokinetics after repeated subcutaneous and intravenous administrations in patients with rheumatoid arthritis and the effect of concomitant methotrexate: an open-label, randomized study. *Clin Ther* **34**:77–90.

Address correspondence to: Abhinav Nath, Department of Medicinal Chemistry, University of Washington, Box 357610, Seattle, WA 98195-7610. E-mail: anath@uw.edu; or William M. Atkins, Department of Medicinal Chemistry, University of Washington, Box 357610, Seattle, WA 98195-7610. E-mail: winky@uw.edu